Preclinical Development

Molecular Cancer Therapeutics

Characterization of the Oncogenic Activity of the Novel *TRIM59* Gene in Mouse Cancer Models

Fatma Valiyeva[1], Fei Jiang[1], Ahmed Elmaadawi[1], Madeleine Moussa[1], Siu-Pok Yee[1], Leda Raptis[2], Jonathan I. Izawa[1], Burton B. Yang[3], Norman M. Greenberg[4], Fen Wang[5], and Jim W. Xuan[1]

Abstract

A novel *TRIM* family member, *TRIM59* gene was characterized to be upregulated in SV40 Tag oncogene–directed transgenic and knockout mouse prostate cancer models as a signaling pathway effector. We identified two phosphorylated forms of *TRIM59* (p53 and p55) and characterized them using purified TRIM59 proteins from mouse prostate cancer models at different stages with wild-type mice and NIH3T3 cells as controls. p53/p55-TRIM59 proteins possibly represent Ser/Thr and Tyr phosphorylation modifications, respectively. Quantitative measurements by ELISA showed that the p-Ser/Thr TRIM59 correlated with tumorigenesis, whereas the p-Tyr-TRIM59 protein correlated with advanced cancer of the prostate (CaP). The function of *TRIM59* was elucidated using short hairpin RNA (shRNA)-mediated knockdown of the gene in human CaP cells, which caused S-phase cell-cycle arrest and cell growth retardation. A hit-and-run effect of *TRIM59* shRNA knockdown was observed 24 hours posttransfection. Differential cDNA microarrray analysis was conducted, which showed that the initial and rapid knockdown occurred early in the Ras signaling pathway. To confirm the proto-oncogenic function of *TRIM59* in the Ras signaling pathway, we generated a transgenic mouse model using a prostate tissue–specific gene (*PSP94*) to direct the upregulation of the *TRIM59* gene. Restricted *TRIM59* gene upregulation in the prostate revealed the full potential for inducing tumorigenesis, similar to the expression of SV40 Tag, and coincided with the upregulation of genes specific to the Ras signaling pathway and bridging genes for SV40 Tag–mediated oncogenesis. The finding of a possible novel oncogene in animal models will implicate a novel strategy for diagnosis, prognosis, and therapy for cancer. *Mol Cancer Ther; 10(7); 1229–40. ©2011 AACR.*

Introduction

The TRIM (TRIpartite Motif) family is an evolutionarily conserved gene family implicated in a number of critical processes including immunity (1–3), antivirus (4–8), proliferation (6, 9), transcriptional regulation (6, 10), neurodevelopment (11, 12), cell differentiation (12), and cancer (13; reviewed in refs. 1, 5, 14, 15). However, the function of most TRIM family members is poorly understood and was surmised only based on computational analysis from their RING finger, B-box, Coiled-Coil (RBCC) sequences. RING (Really Interesting New Gene) domain genes are frequently involved in proteolysis acting as E3 ubiquitin ligases and the ubiquitin–proteasome system in the regulation of numerous cellular processes including cell-cycle regulatory proteins, transcription factors, and signal transducers (6, 15). Antiviral activity associated with the RING finger E3s has been reported in several members of the TRIM gene family, including the HIV restriction factor TRIM5α variant (2, 8) and the disease-associated proteins. B-boxes (1, 2) are domains that bind 1 Zn^{2+}, although their function is unknown. Recent reports show that TRIM members function in microRNA processing (14). A large class of TRIM-NHL proteins that function as a cofactor for the microRNA-induced silencing complex (miRISC; refs. 14, 16) were characterized. TRIM32 activates microRNAs, targets, and ubiquitinylates c-Myc for proteasome-mediated degradation, which prevents self-renewal in mouse neural progenitors (12). An ataxia telangiectasia group D complementing gene (*ATDC*) was reported in most invasive pancreatic cancers upregulated in the Wnt/β-catenin signaling pathway (13).

Because cancer of the prostate (CaP) does not occur naturally in rodents, autochthonous genetically engineered mouse (GEM)-CaP models have been generated (for review, see ref. 17). Currently, the most widely used

Authors' Affiliations: [1]Lawson Health Research Institute, University of Western Ontario, London; [2]Queen's University, Kingston; [3]Sunnybrook Research Institute, Sunnybrook Health Sciences Centre, Toronto, Ontario, Canada; [4]Clinical Research Division, Fred Hutchinson Cancer Research Center, Seattle, Washington; and [5]Institute of Biosciences and Technology, Texas A&M University System Health Science Center, Houston, Texas

Note: Supplementary material for this article is available at Molecular Cancer Therapeutics Online (http://mct.aacrjournals.org/).

Corresponding Author: Jim W. Xuan, Lawson Health Research Institute, 375 South Street, London, ON, N6A 4G5, Canada. Phone: 519-667-6682; Fax: 519-432-7367; E-mail: jim.xuan@lhsc.on.ca

doi: 10.1158/1535-7163.MCT-11-0077

GEM-CaP models all use SV40 Tag[344,456]. We have established 2 GEM-CaP models in which the *PSP94* promoter drives the expression of T/tag to the prostate (18–21): the *PSP94* gene-directed TransGenic Mouse Adenocarcinoma Prostate (PSP-TGMAP) model (18, 21, 22) and the KnockIn Mouse Adenocarcinoma Prostate (PSP-KIMAP) model (19, 20). We conducted a series of cDNA microarray analyses to study upregulated gene profiles (23). One of these upregulated genes, *TRIM59* (NM_025863; 2,858 bp) with unknown function in Tag-induced transgenic mouse models, was chosen for further analysis.

Materials and Methods

For more details, see Supplementary Materials and Methods.

PSP94 gene directed TRIM59, TGMAP, and KIMAP GEM-CaP models, histology, and pathology

A 3.84-kb promoter/enhancer region of the *PSP94* gene was used in all transgenic mouse models for targeted upregulation in the mouse prostate. Protocols for mouse microdissection, anatomic, pathologic, and histologic grading were conducted as previously reported (18–20, 22, 24). Histopathologic classifications were done according to the standard (18–20) and were scored blindly by pathologist (M. Moussa) and at least two other authors independently. All animal experiments were conducted according to the approved University Council of Animal Care.

cDNA microarray (GeneChip; Affymetrix) analysis

Total cellular RNA was extracted using an RNeasy Mini Kit (Qiagen) as previously reported (20, 23). All chip experiments were carried out at the London Regional Genomics Centre. All GeneChips were from Affymetrix: MG_U74Av2, MOE430A, or MOE430 2.0 (23) for mouse and HGU133 Plus 2 for human cell line. Gene expression levels were analyzed using standard softwares.

Semiquantitative, real-time reverse transcriptase PCR (RT-PCR), and Northern blotting were carried out according to reported procedures (20, 23, 25). Real-time PCR was conducted according to the Invitrogen Kit (SYBR GreenER qPCR SuperMix Universal) by the ABI 7900 Real Time PCR System and tested by 3 dilutions of the template cDNA. All oligoprimers used were listed in Supplementary Table S1.

Expression of recombinant GST mouse TRIM59 fusion protein, generating of mouse TRIM59 antibodies

A full-length cDNA clone of mouse *TRIM59* (2,858 bp) was purchased (Invitrogen; MGC IRAV 4017983) and used for cloning into pGEX2T vector (GE-Amersham). All purification procedures of glutathione *S*-transferase (GST) fusion proteins were followed according to the manufacturer's manuals. Approximately 1.5 mg of purified GST–TRIM59 proteins was immuned to rabbit.

Immunohistochemistry

Standard ABC (Avidin Biotin Complex) protocol was conducted as previously reported (21, 22, 24).

Cell culture and ^{32}P labeling in cultured cells

Mouse fibroblast cell line NIH3T3, human prostate cancer cell lines DU145, PC3, LNCaP, and human cell line HEK293 were purchased directly from American Type Culture Collection and maintained in Dulbecco's Modified Eagle's Media (DMEM; Invitrogen/Gibco) with 10% FBS. Numbers of passages of cell culture were minimized by fresh retrieval from original liquid nitrogen stock (<6 months of cultured cells) for the new project. ^{32}P labeling of total cellular phosphoproteins in cultures cells was conducted as per the work of Ausubel and colleagues (25). Labeled proteins were immunoprecipitated with *TRIM*59 antibodies according to immunoprecipitation procedures.

Detection of phosphoprotein by immobilized metal affinity chromatography column

Tissue lysates were first titrated by BioRad protein assay, and all experimental procedures were carried out according to (23) the manufacturer's instructions (from PhosphoProtein Kit, Qiagen and Phosphoprotein Enrichment Kit, Clontech). Samples were taken from every separation procedure (named before, pass, wash, eluate E1, E2 ...). All purified proteins were concentrated by centrifugal ultrafiltration (Ultrfree-0.5, 5KUMWL, Millipore). For immunoprecipitation, protein A column (GE-Amersham) purified *TRIM*59 antibody was coupled and immobilized according to the manufacturer's instructions (Seize Primary Mammalian IP kit).

Establishment of the mouse TRIM59 immunoaffinity column

Approximately 2 mL Protein A column purified *TRIM*59 rabbit antiserum was covalently conjugated to prepacked *N*-hydroxy-succinimide (NHS)-activated Sepharose column (GE-Amersham).

Transient and stable transfection of cultured cells was carried out using Lipofectamine 2000 (Invitrogen/Gibco). Approximately 1×10^6 cells were inoculated in 60-mm Petri dish and transfected with 2 μg of plasmid DNA.

ECL Western blotting was carried out as per protocol by GE-Amersham. Antibodies used were as follows: GST–*TRIM*59#71 and GST–*TRIM*59#72 (dilution of 1:1,000), horseradish peroxidase conjugate anti-rabbit or mouse (CalBiochem; 1:1,000), p-Thr-Polyclonal (Cell Signaling; 1:2,000), and p-tyrosine monoclonal (1:1,000).

ELISA quantification of mouse TRIM59 proteins was followed as previously reported (21) in a 94-well reader (Multiskan EX; Thermo).

Flow cytometry

Flow cytometric cells were stained with propidium iodide according to the protocol of Beckman DNBA Prep Reagents Kit. DNA histograms were analyzed using the EPICS XL-MCL flow cytometer (Beckman Coulter Electronics).

Cell proliferation rate was determined by counting cells in a times course test in 60 mm Petri dishes.

Statistical analysis

Student's *t* tests and 1-way ANOVA were used to analyze the data. All graphs with error bars were generated by Microsoft Excel or SigmaPlot 2000 programs.

Results

Characterization of the novel *TRIM59* gene related to SV40 Tag–induced tumorigenesis in GEM-CaP models

The GeneChip analysis showed that the *TRIM59* gene (NM_025863) was upregulated by 16.84- and 24.07-fold at 20 and 60 weeks (23), respectively, in the KIMAP mice compared with the wild-type (WT) control. These age groups exhibited histologic changes that are representative of tumorigenesis, including prostatic intraepithelial neoplasia (PIN), well-differentiated (WD) CaP, and moderately differentiated (MD) CaP. In contrast, *TRIM59* was downregulated by 0.6-fold in large, poorly differentiated (PD CaP) tumors in the TGMAP model with androgen-independent (AI) and neuroendocrine (NE) carcinoma features within 4 to 8 months of age, which was similar to that induced by SV40 Tag expression (23, 26). Figure 1A shows bioinformatics data for the *TRIM59* gene, including the structure, cDNA, and protein open reading frame (ORF), and hypothetical RBCC domains. Semiquantitative RT-PCR (20, 23) confirmed that *TRIM*59 mRNA was higher in KIMAP tumors than in the WT controls at 20 and 60 weeks of age as well as mouse fibroblast NIH3T3 cells after normalization against glyceraldehyde-3-phosphate dehydrogenase (GAPDH; Fig. 1B). Northern blots hybridized with ^{32}P-dCTP-labeled 250-bp RT-PCR products showed a 2.5-kb mRNA band, which migrated at the predicted size (Fig. 1C).

To characterize the protein product, we generated 2 polyclonal antibodies (Fig. 1A). The first antibody, GST–*TRIM*59#71, was raised against recombinant *TRIM*59 that contained an N-terminal fragment (163 aa) covering several hypothetical RBCC domains. The second antibody, GST–*TRIM*59#72, was raised against recombinant *TRIM*59 that contained the C-terminal fragment (126 aa) that was composed predominantly of *TRIM*59-specific epitope sequences. The *TRIM*59#72 antibody detected a unique or a major band of 53 kDa that was close to the predicted size of 44.77 kDa (403 aa) in Western blots probing lysates from cultured cells (Fig. 2A) and GEM-CaP tissues (Fig. 2D). The N-terminal *TRIM*59#71 antibody recognized multiple bands; however, the same unique band was detected when the antibody was used to probe proteins purified from the *TRIM*59#72 affinity column (see Supplementary Fig. S1).

Immunohistochemical (IHC) staining of GEM-CaP tissues with the *TRIM*59#72 antibody showed positive staining of *TRIM*59 in 5 main grades of hyperplasia, including PIN, WD, MD, and PD CaP, and negative staining in the WT tissue (Fig. 1D and E). We scored by foci the extent of *TRIM59*#72 IHC staining in GEM-CaP mice ($n = 20$). Graph (Fig. 1E) showed nuclear staining in the cell proliferative area; that is, PIN and all cancer foci were significantly higher ($P < 0.01$) than in the cytoplasm. However, there was no difference in cytoplasmic staining with cancer foci (Fig. 1F). The IHC staining intensity for *TRIM*59 was lower in late-stage tumors (PD CaP). *TRIM*59 protein was predominantly expressed in the cytoplasm of cells (Fig. 1D, red arrows). As a control, immunohistochemistry of SV40 Tag showed that the protein localized exclusively in the nucleus (Fig. 1D, black arrows).

Characterization of phospho-*TRIM*59 protein by phosphoprotein affinity IMAC

Because most of the downstream effectors of SV40 Tag are phosphorylated proteins located in the nucleus, including pRB and p53, we first characterized the state of phosphorylation (p-) of *TRIM*59 to show that *TRIM*59 was possibly a downstream effector of SV40 Tag. Using IMAC enrichments, we noticed that the intensity of the phosphorylated 53-kDa band did not change after the lysates were passed through IMAC. Densitometry measurements of the Western blots revealed that only approximately 1/250th of the total cellular protein contained phosphorylated *TRIM*59. Two bands that had a molecular weight of 53 kDa and 55 kDa reacted with the *TRIM*59#72 antibody and were designated as *TRIM*59-p53 and *TRIM*59-p55, respectively (Fig. 2A). We repeatedly observed this result in most of the IMAC experiments, as shown by the elutions from the Qiagen and Clontech purification kits (Fig. 2B). Addition of 0.5×, 1×, and 2× PBS as a competitor to the cell lysates that were loaded onto the IMAC columns blocked the binding of *TRIM*59-p53 and -p55 to the column (Fig. 2A). Whereas the other 3 phosphoproteins immunoreactive to the *TRIM59*#72 antibody, which may be due to overloading of proteins from concentrated IMAC elutions, were less sensitive to the competition (data not shown). We further confirmed this result by adding GST–*TRIM*59#72 as a competing immunogen in the Western blot experiments (data not shown). The ^{32}P labeling of total cellular phosphoproteins in cultured NIH3T3 cells showed that a p-*TRIM*59 band was present after immunoprecipitation using the *TRIM*59#72 antibody immobilized on an agarose gel matrix (Fig. 2C).

Two p-*TRIM*59 forms correlate with tumorigenesis and progression in GEM-CaP mice

We applied the same IMAC column enrichment to GEM tumor tissues (Fig. 2D) obtained from KIMAP mice

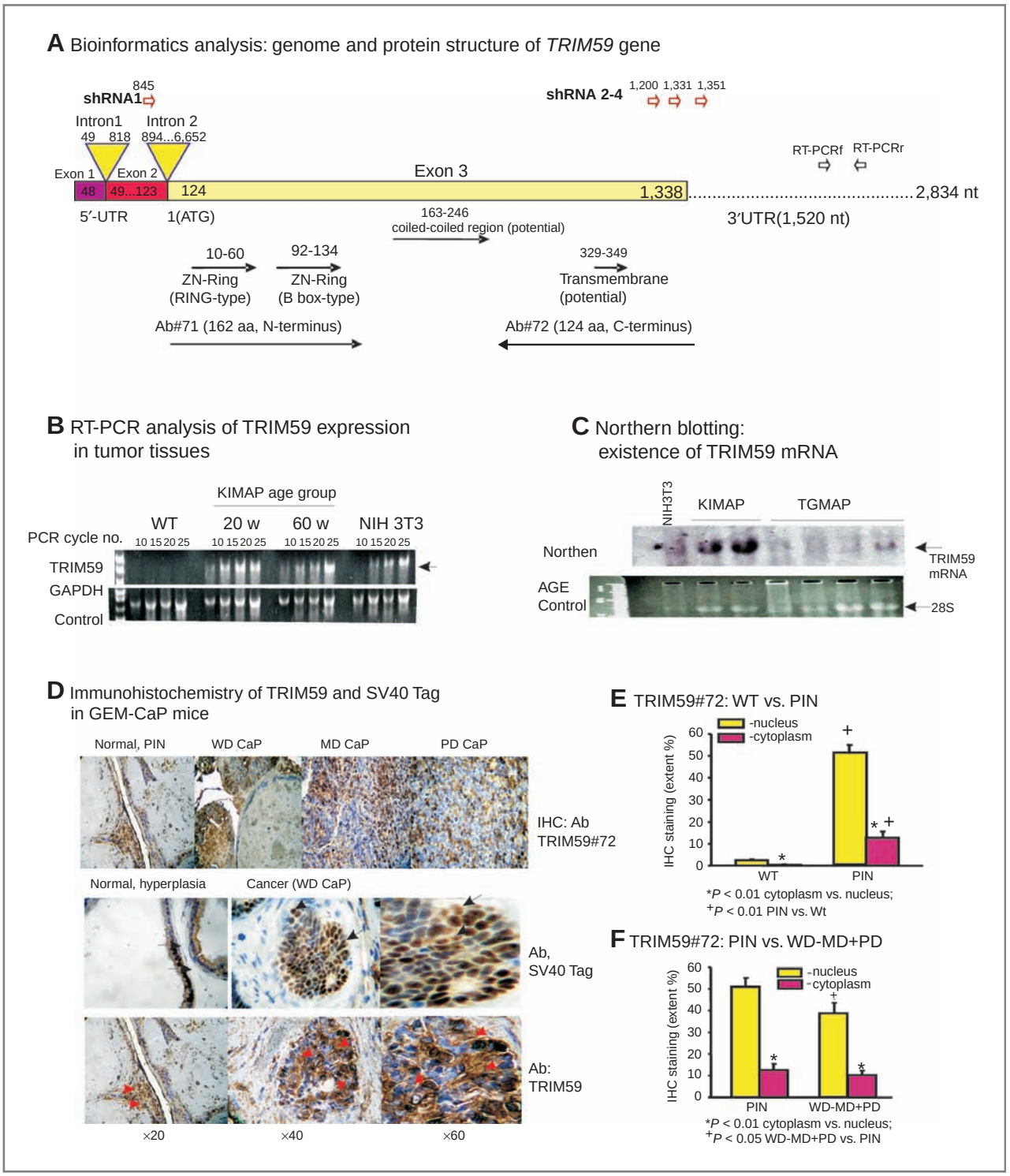

Figure 1. Characterization of a novel *TRIM* family member, *TRIM59* gene. A, summary of *TRIM59* gene structure (top line), cDNA/mRNA structure (second row), the coding region (ORF), 5′- and 3′-UTR, functional domains of RBCC family. Top 4 arrows show positions of 4 shRNAs. Semiquantitative RT-PCR (B) and Northern blotting (C) analyses of *TRIM59* mRNA. Numbers of each lane stand for the PCR cycle numbers. EB-stained Northern agarose gel (second row) as a control. D, comparison of IHC signals of *TRIM59* (*TRIM59#72* rabbit antiserum; 1:1,000 dilution) and SV40 Tag (1:1,000; CalBiochem) in SV40 Tag directed GEM-CaP models, ×20, ×40, ×60. First 4 rows: representative slides of *TRIM59*-IHC in different tumor grades, hematoxylin staining, ×20. (objective, with zoomed camera). Correlation was shown in graphs of E and F. nt, nucleotide.

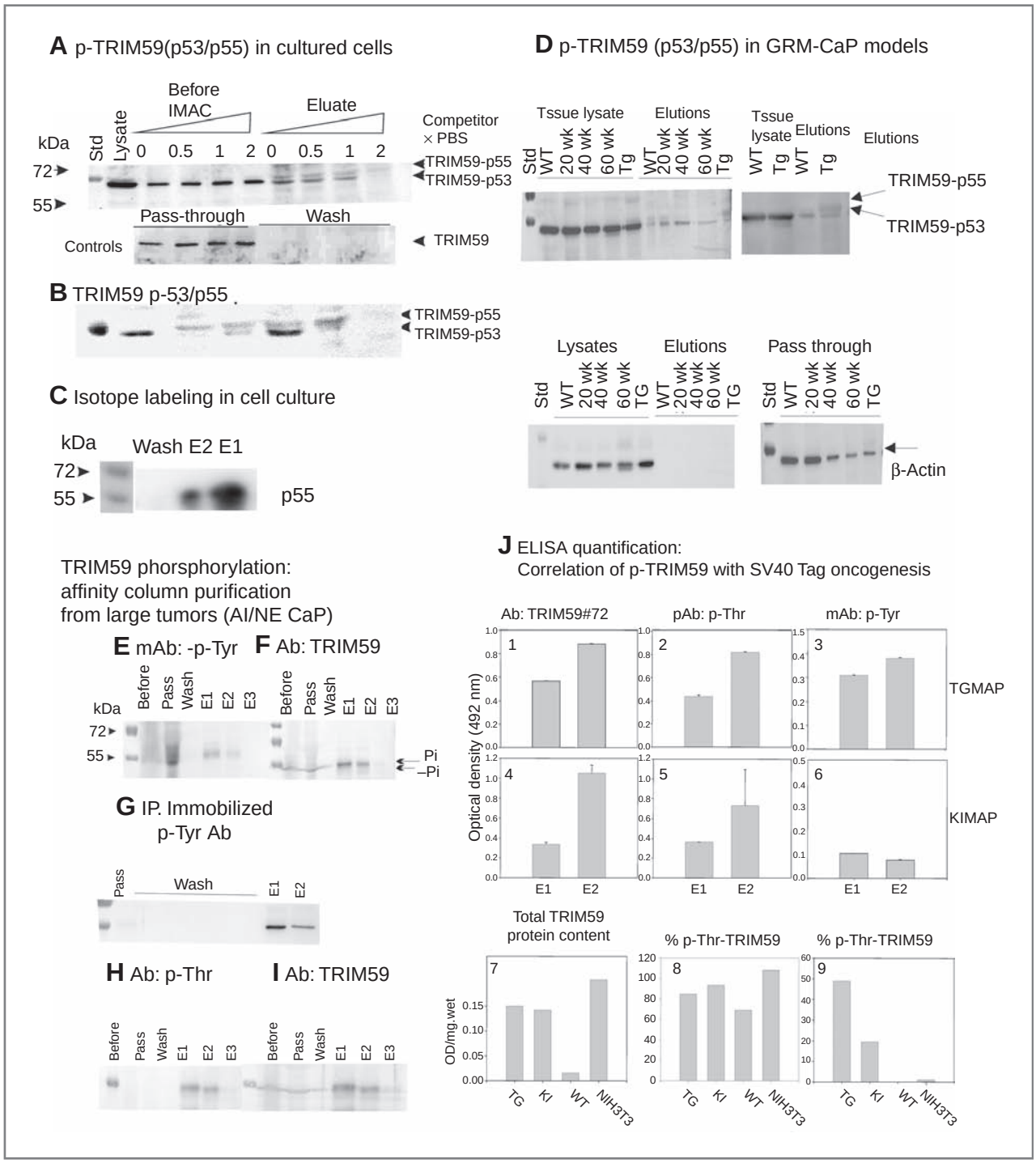

Figure 2. Characterization of p-TRIM59 proteins. A, Western blot analysis of mouse p-TRIM59 proteins by IMAC column purification from NIH3T3 cells and with different IMAC kits by Clontech (B); others were the same but using Qiagen kits. PBS competitors (0, 0.5, 1, and 2 mL of PBS) were added in the lysates. Samples were taken from every separation procedure (named before, pass, wash, eluate E1, E2 . . .). All purified proteins were concentrated by centrifugal ultrafiltration (Ultrfree-0.5, 5KUMWL, Millipore). C, ^{32}P [H_3PO_4] labeling of p-TRIM59 proteins in NIH3T3 cells showing elutions as a result of immunoprecipitation. Correlation of *TRIM*59-p53 and -p55 with tumorigenesis and progression in GEM-CaP models shown by Western blotting (D) of purified p-*TRIM*59 from IMAC column and from affinity column (E–I). J, ELISA quantification of p-TRIM59 proteins. *y*-axis: $OD_{495\ nm}$ normalized by mg (wet weight) of all samples.

with PIN or WD (20 weeks, $n = 12$), MD CaP mice (40 weeks, $n = 11$; 60 weeks, $n = 7$), and TGMAP (TG) mice (late-stage tumors, $n = 5$). The p-*TRIM*59-p53 and -p55 forms were again identified and were similar to those seen in the NIH3T3 cells (Fig. 2D). *TRIM*59-p55 appeared as a weaker band and was found exclusively in large tumors from TGMAP (Fig. 2D). The semiquantitative Western blots showed that the levels of *TRIM*59-p53 in the 20- and 40-week-old KIMAP mice appeared to be higher than those in the 60-week-old age group, TGMAP mice, and WT mice. More protein was loaded in the WT samples to visualize the *TRIM*59 band, as these samples had lower *TRIM*59 levels. Normalized tissue lysates and pass-through fractions were used as controls, as both β-actin and GAPDH are not phosphorylated proteins (Fig. 2D).

To further investigate the *TRIM*59 phosphorylation sites, we purified TRIM59 proteins on an affinity column coupled with the *TRIM*59#72 antibody. We first tested pooled lysates from large TGMAP tumors ($n = 12$) by Western blotting and probed the membranes with 2 different antibodies against p-tyrosine (p-Y; Fig. 2E) and p-threonine (p-T, which stands for all p-S/T proteins; Fig. 2H). As a control, the same blots were reprobed with the *TRIM*59#72 antibody to identify total *TRIM*59 protein (Fig. 2F and I). As shown in Fig. 2E and F, p-Y-*TRIM*59 (Pi) showed slightly higher mobility in SDS-PAGE than the non-phosphor-form (−Pi). The p-T-*TRIM*59 protein had approximately the same mobility as the nonphosphorylated form (Fig. 2H). Densitometry scanning of the blots shown in Fig. 2E versus 2F and 2H versus 2I showed that approximately 30% and 70% of the total p-*TRIM*59 protein were p-Y and p-S/T residues, respectively.

To confirm the specificity of the reprobing test, we used an immobilized p-Y antibody to immunoprecipitate the affinity column purified *TRIM*59 and confirm the p-Tyr antibody reprobing experiment (Fig. 2G). Similarly, we also confirmed that less p-T and p-Y residues of p-*TRIM*59 were detected in the KIMAP mice (20–40 weeks of age; $n = 15$) by carrying out an immunoprecipitation using *TRIM*59#72 immobilized antibody (data not shown).

ELISA quantification shows that *TRIM*59 protein and hyperphosphorylation correlate with SV40 Tag–induced oncogenesis

To quantify the concentration of total *TRIM*59 protein and the p-forms, we established an ELISA protocol. We used *TRIM*59 protein purified on an affinity column from prostate tumors of 10 mice each from the KIMAP and TGMAP models. WT mice and NIH3T3 cells were used as controls. The elution fractions E1 and E2 of the *TRIM*59 protein (as shown in Fig. 2E–I) were tested separately, and p-Y- and p-S/T-*TRIM*59 protein were roughly separated in these first 2 fractions (Fig. 2J2 and J3). The *TRIM*59#72 antibody was used to measure the total *TRIM*59 protein concentration and served as reference for the normalization of all other samples (Fig. 2J7).

The ELISA results showed that the TGMAP mice had the highest levels of Y phosphorylation, which was 2 to 3 times higher than the KIMAP and WT control, and suggested an association with the progression to large, late-stage AI and NE CaP (Fig. 2J9). Moreover, TGMAP and KIMAP displayed higher levels of total *TRIM*59 protein, p-Y-, and P-S/T–phosphorylated *TRIM*59 than WT mice (Fig. 2J7 and J8). Therefore, p-S/T-*TRIM*59 hyperphosphorylation may correlate with SV40 Tag–mediated tumorigenesis. Surprisingly, the NIH3T3 cells displayed a high percentage of p-S/T-*TRIM*59 protein, which may have been due to the high rate of cell proliferation (Fig. 2J8).

*TRIM*59 mRNA knockdown results in S-phase and cell growth retardation

To investigate *TRIM*59 function, we carried out knockdown experiments of *TRIM*59 mRNA expression using a mixture of 4 short hairpin RNA (shRNA) plasmids, which targeted the 5′ end (sh1) and 3′ end (sh2 and sh3) of the human *TRIM*59 ORF as well as the 3′ untranslated region (UTR; sh4). The last shRNA plasmid bound closely to the miR17 target sequence (ref. 27; Fig. 1A). Transient transfection of the human CaP cells and analysis by flow cytometry revealed a statistically significant ($P = 8 \times 10^{-7}$; repeated 20 times) decrease in the percentage of S-phase cells for both the DU145 and PC3 cells compared with other phases of the cell cycle (sub-G_1, >G_1, G_0–G_1, S, G_2–M, 3N, and 4N) and the control (pSilencer neo-negative, from Ambion kit; Fig. 3A and Table 1). All 5 cell division cycle (CDC) phases were decreased, except sub-G_1 phase cells ($P > 0.05$). Stable transfectant clones ($n = 7$; Fig. 3B and Table 2) also showed cell-cycle arrest in the S-phase ($P = 0.002$).

Cell proliferation assessment showed significant growth retardation (50%–30% reduction compared with control) in both transient (Fig. 4A) and stable transfectants (Fig. 4B). shRNA knockdown of TRIM59 in a slow growing human CaP cell line (LNCaP) caused significant cell death (data not shown). Real-time RT-PCR quantification of 3 dilutions of cDNA templates showed that *TRIM*59 mRNA was decreased by 50% 24 hours after the transient transfection in DU145 and PC3 cells and returned to normal levels 48 hours after the transfection (Fig. 4C). Similar results were observed in all of the DU145 and PC3 stable transfectants (Fig. 4F). Both pSilencer-neg and pcDNA plasmids were used as negative controls and the experiments were repeated 4 times.

A hit-and-run effect of targeting *TRIM*59 in the Ras signalling pathway suggests it is an early and rapid signal transmitter

We hypothesized that due to a hit-and-run effect, the effects on the original signal transduction targets of *TRIM*59 could only be detected at 24 hours posttransient knockdown (Tr24), but not at later time points or in the stable transfectants (S), despite the fact that they had the

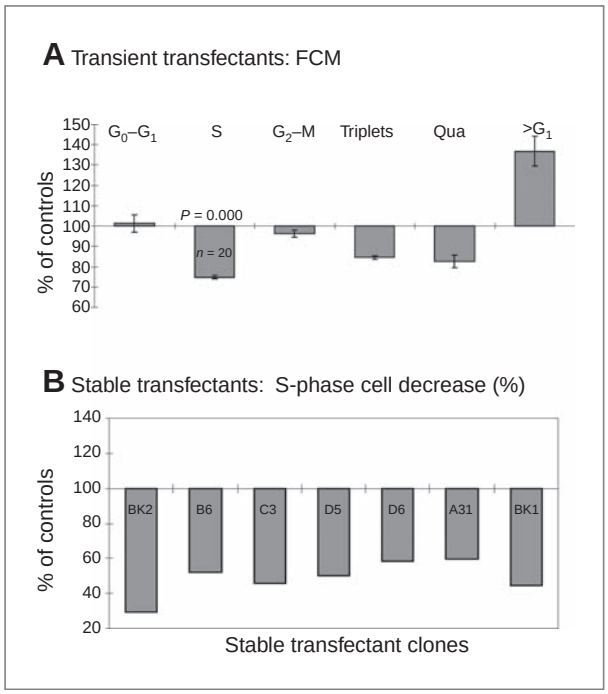

Figure 3. shRNA knockdown of *TRIM59* gene in human prostate cancer cells resulted in S-phase arrest. Graphs show results of flow cytometry of transient (A) and stable transfectant clones (B, neo^R, $n = 7$ names of clones marked) of *TRIM59* shRNA (sh1–4) plasmid mixture. All graphs show percentages of control transfection. Error bars ± SD. FCM, flow cytometry.

same phenotype. Because *TRIM59* function is critical for cell survival, we only observed a rapid and transient, less than a 50% reduction in shRNA-mediated knockdown of *TRIM59* expression. We only detected marginal reductions of *TRIM59* protein and hyperphosphorylation in Western blot experiments (data not shown), which may be due to *TRIM59* acting as an early and rapid signal transmitter.

We carried out a differential GeneChip experiment using the S and Tr24 samples. The results of the GeneChip confirmed the hit-and-run hypothesis and showed that *TRIM59* mRNA had a 16% reduction compared with the S group. Figure 4E shows 2 kinds of differential GeneChip analyses. The first analysis was the Unique Tr24–S gray zone ($n = 43$), which screened for genes in the Tr24 group that had a unique decrease of 1.5-fold compared with genes in the S group, which only had a ±10% change (gray zone). The second analysis was the Unique Tr24-S D ($n = 59$), which assessed differences greater than 1.3-fold between the genes of the Unique Tr24 and S groups (either decreased or increased). Both of these 2 differential screening analyses, which are shown by Unique Tr24-S (gray zone) (Fig. 4F2) and Unique Tr24-S D function group maps (Fig. 4F3), exhibited a unique and rapid downregulation of *K-Ras* oncogenes, such as K-Ras and RasSF5. In contrast, only Ras downstream genes (e.g., phosphoinositide-3-kinase/Akt and Rho) were observed in the S group (Fig. 4F1). Supplementary Fig. S2 provides the detailed lists and GeneChip heat maps.

TRIM59 has proto-oncogenic activity in a transgenic mouse model test

To test the oncogenic activity of *TRIM59* in the Ras/SV40 Tag signaling pathways, a transgenic mouse prostate model was developed, which used a prostate tissue–specific gene promoter of the *PSP94* gene to directly upregulate mouse *TRIM59* gene expression (Fig. 5A). Transgenic upregulation of *TRIM59* was confirmed by RT-PCR using primer pairs of FLAG (3′ end) and a 300-bp upstream oligonucleotide (Fig. 5B and Supplementary Table S1). The GeneChip also confirmed *TRIM59* gene upregulation (2.24-fold). Four F0 breeding lines, which were bred until F3 with 60 male mice, were established. Histopathologic analysis was conducted on 15 mice that were 100 to 110 days old from all 4 established breeding lines (Fig. 5C, F0–F3 until 12 months of age). The results of the hematoxylin and eosin staining of the prostate samples showed that 3 mice developed WD CaP, which was mostly in the dorsolateral prostate and the region that is most sensitive to carcinogenesis in rodents (28), 6 mice developed low- to high-grade PIN, and 6 mice were normal. Atrophic glands were often observed (Fig. 5D). PSP94-*TRIM59* mice (110-day-old) also showed invasion (invasive carcinoma, IC) of the surrounding glands and the formation of fused glands (Fig. 5C; WD CaP-IC). Figure 4C shows a moderately differentiated tumor with the formation of multiple small and fused glands

Table 1. Statistical analysis of flow cytometry of transient transfectants

	G_0–G_1	S	G_2–M	3N	4N	>G_1
Control average	52.24%	7.15%	17.59%	6.00%	6.58%	10.44%
TRIM59sh average	52.92%	5.35%	16.95%	5.07%	5.44%	14.28%
t test	0.69619665	8.7763E-07	0.2115273	0.0327041	0.041101723	0.0630796

NOTE: S-phase cell proportion (by content percentage) was repeatedly ($n = 12$) found to be highly significant ($P = 10^{-7}$), lower than all other CDC cells groups: sub-G_1 (>G_1), G_0–G_1, S, G_2–M, 3N (triplets), and 4N (qua), as compared with the control (pSilencer 4.1 neo-negative, from Ambion kit).

Table 2. Statistical analysis of flow cytometry of stable transfectants

	G_0–G_1	S	G_2–M	3N	4N	>G_1
Control average	57.10%	13.45%	16.00%	6.12%	5.41%	1.93%
TRIM59sh average	47.21%	7.57%	22.28%	8.06%	9.73%	5.14%
t test	0.3021	0.00249	0.2115	0.2902	0.3239	0.4170

NOTE: S-phase cell proportion (by content percentage) was repeatedly ($n = 12$) found to be highly significant ($P = 10^{-7}$), lower than all other CDC cells groups: sub-G_1 (>G_1), G_0–G_1, S, G_2–M, 3N (triplets), and 4N (qua), as compared with the control (pSilencer 4.1 neo-negative, from Ambion kit).

from mice that were 170 to 200 days old ($n = 3$). The PSP94-*TRIM*59 mice developed poorly differentiated CaP and comedocarcinoma, which had features of NE (small cell carcinoma) and central necrosis. Of 26 PSP94-*TRIM*59 mice analyzed, 6 mice (23%) had cancer predominantly in the dorsolateral prostate with WD CaP, whereas 15 (57.7%) of the mice showed a normal prostate structure.

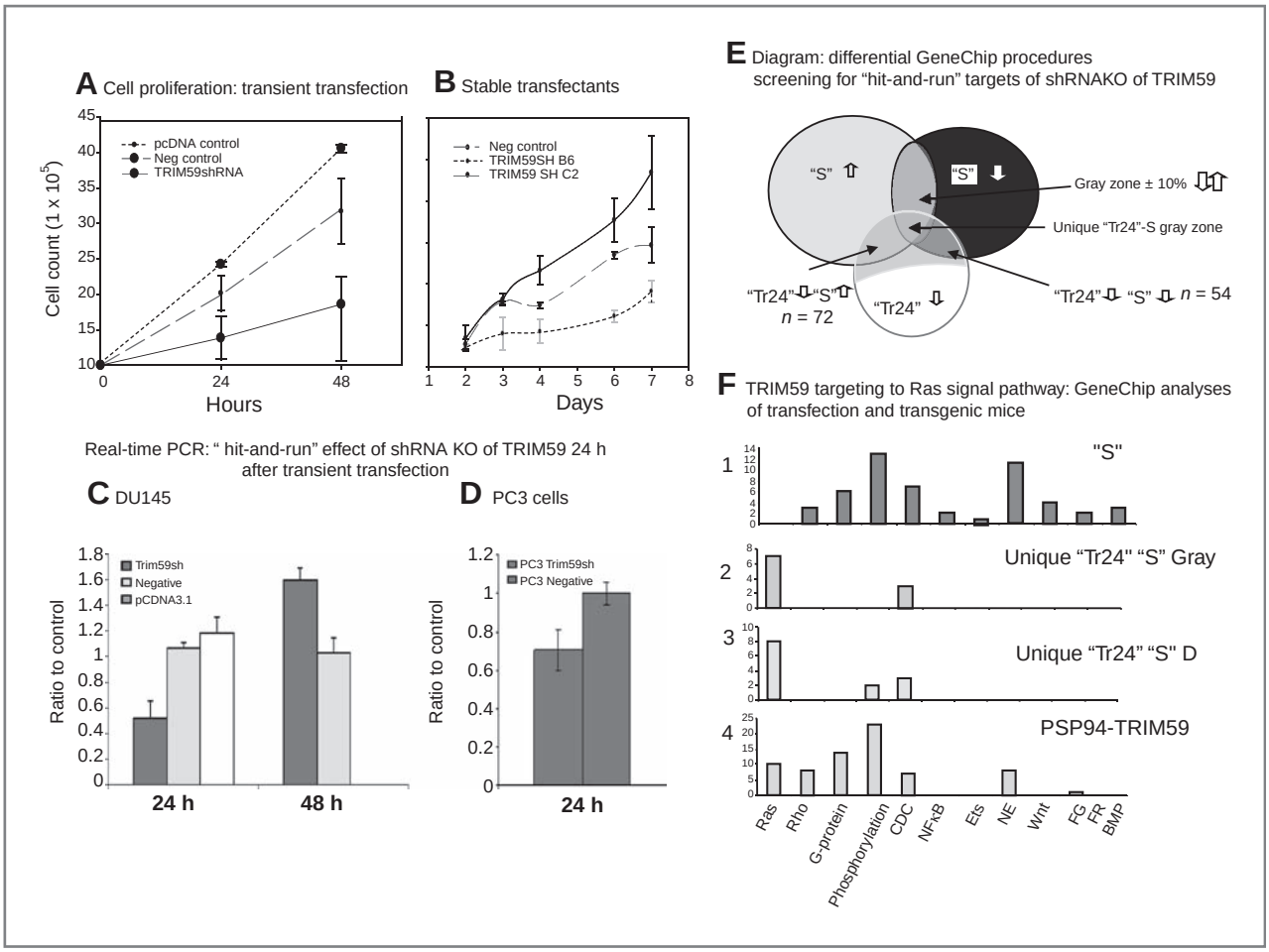

Figure 4. shRNA knockdown of *TRIM*59 gene in human prostate cancer cells. Cell proliferation rate shown in determination of both transient transfection (A; 24 and 48 hours) and stable transfectant clones (B; #B6 and #C2) of *TRIM*59 shRNA. C and D, real-time PCR quantification of hit-and-run effects of *TRIM*59 shRNA knockdown only 24 hours after transient transfection in both DU145 (C) and PC3 (D) cells. Error bars ± SD. WT mouse prostate, NIH3T3, and GAPDH were used as controls. Oligonucleotide DNA primer pairs are listed in Supplementary Table S1. E and F, *TRIM*59 functional targets in Ras signal pathway by GeneChip analyses. E, diagram shows differential GeneChip analysis on the hit-and-run effect of in shRNA 24 hours after transient transfection (unique Tr24). Gray zone: change (±10%). F, bar graphs showing the results of differential GeneChip screening comparison of the contents of gene functional groups in *TRIM*59 shRNA knockdown (F1–3) with transgenic PSP94 *TRIM*59 mice (F4).

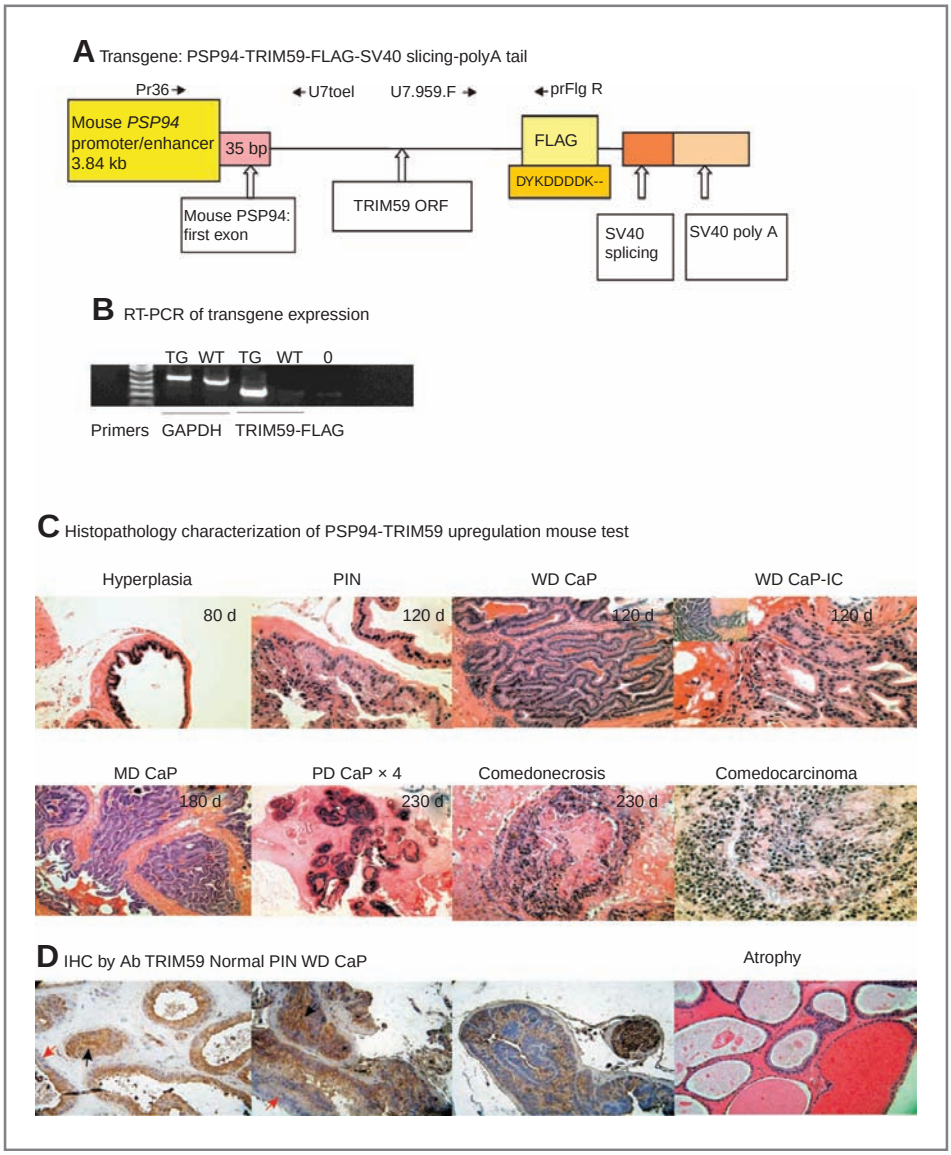

Figure 5. Transgenic mouse test of the proto-oncogenic activity of *TRIM59*. A, structure of PSP-*TRIM59* transgene: the whole *TRIM59* ORF was modified by insertion of a FLAG (DYKDDDDK), an immunoepitope tag, and followed by SV40 small t-splicing and poly A tail sequences. Genotyping for 4 breeding lines were determined by 2 sets of primers (arrows; Supplementary Table S1) by a quick tail PCR procedure (18–20). B, RT-PCR demonstration of PSP-*TRIM59* transgene expression. C, histopathologic show of tumorigenesis and progression (by days) of PSP94-*TRIM59* transgenic mice. All panels were ×20, except inlet ×10, PD CaP ×4, ×20, ×40. D, IHC staining with antibody *TRIM59*#72, ×20. Arrows indicate glands with negative (red) and positive (black) staining.

The transgenic *TRIM59* model confirmed *TRIM59* function in the Ras/Braf/MEK/ERK signaling pathway with possible links to the SV40 Tag/pRB/p53 pathway

To further characterize the oncogenic nature of PSP94-*TRIM59* transgenic mice, a GeneChip analysis was conducted using WT mice as references. The *TRIM59* gene was upregulated by 2.24-fold in the GeneChip analysis. Of the genes that were upregulated by 10-fold, the majority of them (68 of 201, 50.7%) were previously described tumor markers, which confirmed that the PSP-*TRIM59* model was a valid cancer model (Supplementary Fig. S3). The high proportion of immune responsive genes (26 of 201, 19.4%) may account for the low tumor incidence and slow growth rate of CaP in PSP94-*TRIM59* mice, which is similar to that observed in the KIMAP model (19, 20).

In PSP94-*TRIM59* mice, we also verified that the *TRIM59* gene functioned in the Ras signaling pathway. The more intense staining of *TRIM59* protein by immunohistochemistry was predominantly found in the cytoplasm of cells located in the cell proliferative area of PIN and WD CaP foci (Fig. 5C), whereas only 10% of the cells showed *TRIM59* nuclear staining (30 of 323). It is important to note that the Ras/Braf/MEK/ERK signaling pathways reside either near the cell membrane or in the cytoplasm, which is in contrast to the nuclear location of the SV40 Tag/pRB/p53 pathway proteins. However, both pathway families regulate cell division and proliferation (29).

As shown in Fig. 4F4, the genes upregulated by 10-fold and most of the genes upregulated by 2- to 10-fold were related to the Ras signaling pathway ($n = 66$). For example, Rho factors and G proteins comprised 38.4% (24 of

66) of the total genes in these groups. Supplementary Figure S3 shows the heat maps for the genes in the list. As a control, the same GeneChip analysis conducted on PSP94-SV40 Tag–directed GEM-CaP models revealed that most of the gene profiling related to abnormality of the CDC checkpoint system and chromosome instability (20, 23).

However, we identified exceptions to these observations and showed that some genes involved in both the Ras/Braf/MEK/ERK and SV40 Tag/pRB/p53 pathways were upregulated in the PSP94-*TRIM*59 mice (Supplementary Table S2). Real-time RT-PCR experiments were carried out on 7 Ras-related genes (*Rac2*, *Pla2g2a*, *Fos*, *Gpr120*, *Gpr18*, *Sgpp2*, and *Styk1*), 5 SV40 Tag effector genes (*Rbbp4*, *Rbbp8*, *Trp53bp1*, *P107*, and *Ccnb1-rs1*), and 1 NE-CaP marker gene (chromogranin, *ChgA*). Prostate samples were tested from 3 GEM-CaP models, including hybrids of F1 (KIMAP × PSP94-*TRIM*59), using the WT mice as controls. Figure 6 shows that Ras-related genes were upregulated in PSP94-*TRIM*59 and had higher expression levels than those in the KIMAP or hybrids of PSP94-*TRIM*59 × KIMAP mice, with the exception of bridging genes such as *Rac2* and *GPR*s. All Tag effectors were higher than either PSP94-*TRIM*59 or the hybrids of PSP94-*TRIM*59 × KIMAP, with the exception of the bridging genes *Ccnb*, *P107*, and *Rbbp*s, indicating a dominant effect over Ras-related genes.

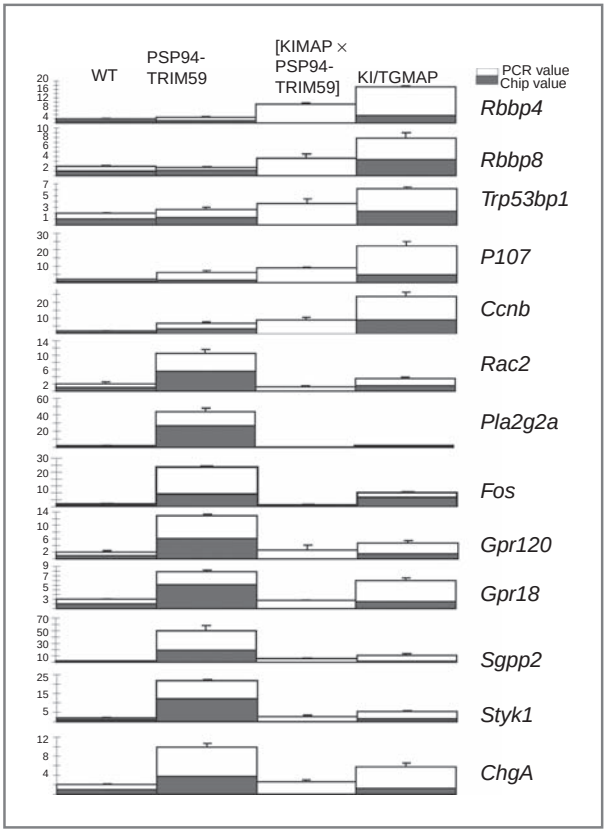

Figure 6. Real-time PCR verification of GeneChip results and determination of expression of bridging molecules between SV40 Tag-GEM-CaP and PSP-*TRIM*59 (Ras) models. Stack bars indicate fold changes as shown in GeneChip list and real-time PCR values. Chip values for F1[PSP94-*TRIM*59 × KIMAP] were not available.

Discussion

In this study, a novel TRIM family member, the *TRIM*59 gene was originally screened for upregulation and association with the SV40 Tag oncogene–mediated tumorigenesis in GEM-CaP models. As with all downstream effectors from Ras and SV40 Tag oncogene families, *TRIM*59 function target still involved in S-phase and cell proliferation regulation.

However, we found that the initial function of TRIM59 may have possibly targeted the Ras oncogene signal pathway. We hypothesize that a mechanism should exist linking between *Ras* and *SV40 Tag/pRB/p53* oncogene signal pathways, one of which is possibly through a new *TRIM*59 signal transduction route (diagram shown in Supplementary Fig. S4). The mechanism coordinating between 2 large oncogene signal pathways is still not clear, in which the RING domain ubiquitinase activities will be involved (15). We assume that *TRIM*59 cytoplasm (p-S/T) and *TRIM*59 nucleus (p-Y) are present in Ras and SV40 Tag/pRb–related signal pathways separately. By ELISA quantization along with characterization by 2 kinds of phosphoprotein antibodies (p-S/T, p-Y), we showed that p-S/T-*TRIM*59 hyperphosphorylation is correlated with the SV40 Tag–initiated tumorigenesis and is then maintained at a relatively stable level during further tumor progression (WD-MD CaP).

One of the most important evidence supporting *TRIM*59 function in Ras signal pathway is the cytoplasmic location of the *TRIM*59 expression, especially in low-grade tumorigenesis stage. SV40 Tag/pRB/p53 are all normally or mostly expressed in the nucleus, whereas Ras/Braf/MEK/ERK reside near the cell membrane or cytoplasm, which both regulates proliferation and differentiation (29). *TRIM*59 expression upregulation, especially the p-Y hyperphosphorylation, increased in the nucleus mostly in MD-PD CaP stage. All other signal pathways with connections with *TRIM*59 knockdown or upregulation (e.g., Wnt-β-catenin, BMP-SMAD, IGF, etc. shown in Fig. 4F and Supplementary Figs. S2 and 3) were initially or majorly expressed in the cytoplasm. In a recent report, Ras and pRb functionally interact, despite their geographical distance, resolving a signaling network involved in cellular senescence and tumor suppression (29). Finally, GeneChip analyses on the PSP94-*TRIM*59 upregulation transgenic mouse test also confirmed that genes related to Ras signal pathway are the most significant upregulated group.

Because *TRIM*59 is an early signal transmitter, we investigated 291 human cancer cases and showed *TRIM*59 upregulation in the cytoplasm in all 37 tumor types (29). Further evidence is also from the hit-and-run effect of *TRIM*59 gene function, which may implicate

*TRIM*59 as a rapid signal transmitter in Ras signal pathway. Probably due to this rapid effect, results of our Western blotting semiquantitative test on levels of *TRIM*59 and p-*TRIM*59 proteins in shRNA knockdown cells and in PSP94-*TRIM*59 mice were marginal (data not shown).

In transgenic mice test, *TRIM*59 significantly revealed its full potential in the tumor progression to NE CaP (the comedocarcinoma) differentiation. As with *Ras* and *Myc* oncogenes, *TRIM*59 function may be involved in S-phase and cell proliferation regulation. We show that the TRIM59, except Ras and c-Myc, plays an important physiologic role and that only a few of these proto-oncogenes can induce cancer in the transgenic mouse test.

Ras mutations are among the most frequent alterations in human cancers that lead to approximately 30% of all human cancers with expression of constitutively active Ras proteins, so it is critical to understand the effector pathways downstream of oncogenic Ras leading to transformation. Our new finding indicates that there are more issues than mutation issues of the Ras signal pathway in tumorigenesis and progression, as we found that a novel *TRIM*59 gene as a proto-oncogene can affect both Ras and RB (SV40 Tag oncogene target) signal pathways just by up/downregulation of its function in DNA synthesis (S-phase).

Disclosure of Potential Conflicts of Interest

No potential conflicts of interest were disclosed.

Grant Support

This work was supported by grants from the Canadian Institute of Health Research (MOP-77684 to J.W. Xuan), NIH-NCI (2 U01 CA084296-06 to N.M. Greenberg, F. Wang, and J.W. Xuan), and the Ontario Institute of Cancer Research (07NOV-52 to J.W. Xuan).

The costs of publication of this article were defrayed in part by the payment of page charges. This article must therefore be hereby marked *advertisement* in accordance with 18 U.S.C. Section 1734 solely to indicate this fact.

Received February 8, 2011; revised April 8, 2011; accepted April 25, 2011; published OnlineFirst May 18, 2011.

References

1. Ozato K, Shin DM, Chang TH, Morse HC III. TRIM family proteins and their emerging roles in innate immunity. Nat Rev Immunol 2008;8:849–60.
2. James LC, Keeble AH, Khan Z, Rhodes DA, Trowsdale J. Structural basis for PRYSPRY-mediated tripartite motif (TRIM) protein function. Proc Natl Acad Sci U S A 2007;104:6200–5.
3. Keeble AH, Khan Z, Forster A, James LC. TRIM21 is an IgG receptor that is structurally, thermodynamically, and kinetically conserved. Proc Natl Acad Sci U S A 2008;105:6045–50.
4. Si Z, Vandegraaff N, O'hUigin C, Song B, Yuan W, Xu C, et al. Evolution of a cytoplasmic tripartite motif (TRIM) protein in cows that restricts retroviral infection. Proc Natl Acad Sci U S A 2006;103:7454–9.
5. Ellis J, Hotta A, Rastegar M. Retrovirus silencing by an epigenetic TRIM. Cell 2007;131:13–4.
6. Gack MU, Shin YC, Joo CH, Urano T, Liang C, Sun L, et al. TRIM25 RING-finger E3 ubiquitin ligase is essential for RIG-I-mediated antiviral activity. Nature 2007;446:916–20.
7. Wolf D, Goff SP. TRIM28 mediates primer binding site-targeted silencing of murine leukemia virus in embryonic cells. Cell 2007;131:46–57.
8. Yap MW, Nisole S, Lynch C, Stoye JP. Trim5alpha protein restricts both HIV-1 and murine leukemia virus. Proc Natl Acad Sci U S A 2004;101:10786–91.
9. Short KM, Cox TC. Subclassification of the RBCC/TRIM superfamily reveals a novel motif necessary for microtubule binding. J Biol Chem 2006;281:8970–80.
10. Lerner M, Corcoran M, Cepeda D, Nielsen ML, Zubarev R, Ponten F, et al. The RBCC gene RFP2 (Leu5) encodes a novel transmembrane E3 ubiquitin ligase involved in ERAD. Mol Biol Cell 2007;18:1670–82.
11. Balastik M, Ferraguti F, Pires-da SA, Lee TH, varez-Bolado G, Lu KP, et al. Deficiency in ubiquitin ligase TRIM2 causes accumulation of neurofilament light chain and neurodegeneration. Proc Natl Acad Sci U S A 2008;105:12016–21.
12. Schwamborn JC, Berezikov E, Knoblich JA. The TRIM-NHL protein TRIM32 activates microRNAs and prevents self-renewal in mouse neural progenitors. Cell 2009;136:913–25.
13. Wang L, Heidt DG, Lee CJ, Yang H, Logsdon CD, Zhang L, et al. Oncogenic function of ATDC in pancreatic cancer through Wnt pathway activation and β-catenin stabilization. Cancer Cell 2009;15:207–19.
14. Loedige I, Filipowicz W. TRIM-NHL proteins take on miRNA regulation. Cell 2009;136:818–20.
15. Deshaies RJ, Joazeiro CAP. RING domain E3 ubiquitin ligases. Ann Rev Biochem 2009;78:399–434.
16. Hammell CM, Lubin I, Boag PR, Blackwell TK, Ambros V. nhl-2 modulates microRNA activity in *Caenorhabditis elegans*. Cell 2009;136:926–38.
17. Abate-Shen C, Shen MM. Mouse models of prostate carcinogenesis. Trends Genet 2002;18:S1–5.
18. Gabril MY, Onita T, Ji PG, Sakai H, Chan FL, Koropatnick J, et al. Prostate targeting: PSP94 gene promoter/enhancer region directed prostate tissue-specific expression in a transgenic mouse prostate cancer model. Gene Ther 2002;9:1589–99.
19. Duan WM, Gabril MY, Moussa M, Chan FL, Sakai H, Fong GH, et al. Knock-in of SV40 Tag oncogene in a mouse adenocarcinoma of the prostate (KIMAP) model demonstrates advantageous features over the transgenic model. Oncogene 2005;24:1510–24.
20. Gabril MY, Duan WM, Wu GJ, Moussa M, Izawa JI, Panchal CJ, et al. A novel knock-in prostate cancer model demonstrates biology similar to that of human prostate cancer and suitable for preclinical studies. Mol Ther 2005;11:348–62.
21. Van Huizen I, Wu GJ, Moussa M, Chin JL, Fenster A, Lacefield JC, et al. Establishment of a serum tumor marker for pre-clinical trials of mouse prostate cancer models. Clin Cancer Res 2005;11:7911–9.
22. Xuan JW, Bygrave M, Jiang HY, Valiyeva F, Dunmore-Buyze J, Holdsworth DW, et al. Functional neo-angiogenesis imaging of genetically engineered mouse prostate cancer using three-dimensional power Doppler ultrasound. Cancer Res 2007;67:2830–9.
23. Guo C, Wu GJ, Chin J, Bauman GS, Moussa M, Wang F, et al. Bub1 up-regulation and hyper-phorsphorylation promote malignant transformation in SV40 Tag-induced mouse models. Mol Cancer Res 2006;4:957–69.
24. Wirtzfeld LA, Wu GJ, Bygrave M, Yamasaki Y, Sakai H, Moussa M, et al. Three-dimensional ultrasound micro-imaging for preclinical studies using a transgenic prostate cancer mouse model. Cancer Res 2005;65:6337–45.

25. Ausubel FM, Brent R, Kingston RE, Moore DD, Seidman JG, Smith JA, et al. Current protocols in molecular biology. New York: John Wiley & Sons. Inc; 2002.
26. Kasper S, Sheppard PC, Yan Y, Pettigrew N, Borowsky AD, Prins GS, et al. Development, progression and androgen-dependence of prostate tumors in probasin-large T antigen transgenic mice: a model for prostate cancer. Lab Invest 1998;78:319–33.
27. Shan S, Lee DY, Deng Z, Shatseva T, Jeyapalan Z, Du WW, et al. MicroRNA MiR-17 overexpression retards tissue growth and represses fibronectin expression. Nat Cell Biol 2009;11:1031–8.
28. Shappell SB, Thomas GV, Roberts RL, Herbert R, Ittmann MM, Rubin MA, et al. Prostate pathology of genetically engineered mice: definitions and classification. The consensus report from the Bar Harbor meeting of the Mouse Models of Human Cancer Consortium Prostate Pathology Committee. Cancer Res 2004;64:2270–305.
29. Shamma A, Takegami Y, Miki T, Kitajima S, Noda M, Obara T, et al. Rb regulates DNA damage response and cellular senescence through E2F-dependent suppression of N-Ras isoprenylation. Cancer Cell 2009;15:255–69.